Wind Turbine Aeroelastic Stability in OpenFAST

Journal of Physics: Conference Series **2767** (2024) 022018 doi:10.1088/1742-6596/2767/2/022018

Wind Turbine Aeroelastic Stability in OpenFAST

Pietro Bortolotti[1], Mayank Chetan[1], Emmanuel Branlard[2], Jason Jonkman[1], Andy Platt[1], Derek Slaughter[1], and Jennifer Rinker[3]

[1]National Renewable Energy Laboratory, Golden CO, 80401, USA
[2]University of Massachusetts, Amherst, MA, USA
[3]DTU Wind Energy, Roskilde, DK-4000, Denmark

E-mail: pietro.bortolotti@nrel.gov

Abstract. Wind turbines are growing in size and increasingly suffer from aeroelastic instabilities. Unfortunately, numerical models often show inconsistent results during verification studies. We address this gap by first introducing novel linearization capabilities within the open-source aero-hydro-servo-elastic framework OpenFAST. Next, a code-to-code benchmark study is presented that compares modal parameters between OpenFAST and HAWCStab2 for a land-based version of the International Energy Agency 15-MW reference wind turbine modeled with quasi-steady aerodynamics. The two solvers are in strong agreement except for discrepancies in the second rotor flapwise modes. The differences are attributed to the torsional flexibility of the tower, which is assumed torsionally stiff in the OpenFAST model. Work is ongoing to close this modeling gap. The aeroelastic stability of a low-specific-power land-based wind turbine is also investigated. The impact of design choices is discussed, highlighting how narrow the margins are between a stable design and an unstable design.

1 Introduction

Wind turbines are growing in size, and their structures are increasingly compliant. Lighter and more slender rotors and towers reduce costs, improve visual aesthetics, and help alleviate logistical constraints [1]. However, recent field experiments have shown that wind turbines are at the boundary of aeroelastic stability, with a growing concern on blade edgewise and torsional modes [2]. Ideally, these potential instabilities would be accounted for during the design phase. Unfortunately, numerical models have often shown inconsistent results during verification studies [3, 4]. Strong sensitivities to the highly nonlinear blade torsional deformations and unsteady rotor aerodynamic effects have been described, and the more complex, but also more realistic, cases have generated unsatisfactory comparisons.

Over the years, multiple tools have been developed to analyze aeroelastic stability of wind turbine blades, many starting from the Theodorsen theory [5]. For instance, Lobitz [6] investigated the flutter behavior of the WindPACT blade, which is 33 m long and powers a 1.5 MW rotor, concluding that the flutter speed was approximately twice the rated rotor speed. As blades have grown longer and more flexible, the studies available in literature registered a reduction in both flutter speeds and flutter margins [7, 8, 9]. Recently, Kelley and Paquette [10] added edgewise aerodynamic terms to the BLade Aeroelastic Stability Tool (BLAST) model implemented at Sandia National Laboratories but did not notice a change in the solutions of a 100-m blade. Chetan et al. [11] used the same formulation to investigate multiple blades for upwind three-bladed and downwind two-bladed rotors, concluding that the former suffer from edgewise instabilities more than the latter, which are characterized by a wider

blade chord distribution that helps generate higher edgewise stiffness. The authors also found that some of their 200-m long blade designs might violate flutter constraints.

In parallel to the models based on the Theodorsen theory, the tool HAWCStab2 has been developed at the Technical University of Denmark (DTU) [12, 13, 14]. HAWCStab2 uses the multi-blade coordinate transformation method [15] and performs the analytical linearization of the full wind turbine system modeled in a co-rotational formulation. While publicly available literature suffers from a general lack of thorough validation studies in the area of wind turbine stability, HAWCStab2 has shown good agreements to field experiments [2].

An alternative approach has been described in Bottasso and Cacciola [16] and Riva et al. [17], where a numerical wind turbine model is excited to identify a single-input/single-output periodic reduced model from the recorded response. The full Floquet theory is then performed on the reduced-order model. This approach overcomes the assumption of isotropic rotors adopted by the multi-blade coordinate transformation method, but also adds layers of complexity.

The two families of approaches have been applied to investigate the aeroelastic stability of a variety of wind turbine rotor configurations, with a recurring focus on blades characterized by passive load alleviation technologies such as backward sweep [13] and bend-twist coupling [18, 19].

This work focuses on this area of growing interest by first introducing novel linearization capabilities within the open-source aero-hydro-servo-elastic framework OpenFAST [20], adopting its geometrically exact beam model BeamDyn to model the elastic response of the blades. The OpenFAST release v3.5.3 is used in this work. Next, a code-to-code benchmark study is presented comparing modal parameters between OpenFAST and HAWCStab2 for the 15-MW International Energy Agency (IEA) reference wind turbine (IEA15MW) [21]. Finally, the stability of a low-specific-power land-based wind turbine designed during the Big Adaptive Rotor (BAR) project is investigated [1]. The impact of design choices on the aeroelastic stability of a wind turbine representing state-of-the-art land-based machines is discussed. The paper closes with recommendations for future work.

2 Numerical models for the aeroelastic stability analysis

We begin by introducing the concept of linearization of a nonlinear system before presenting the aspects specific to OpenFAST and HAWCStab2.

2.1 General concepts

A nonlinear system can typically be represented using a state equation and an output equation:

$$\dot{\boldsymbol{x}} = \boldsymbol{X}(\boldsymbol{x}, \boldsymbol{u}), \qquad \boldsymbol{y} = \boldsymbol{Y}(\boldsymbol{x}, \boldsymbol{u}) \tag{1}$$

where $\boldsymbol{x}$ is the vector of states describing the system (e.g., elastic degrees of freedom describing the motion of the wind turbine), $\boldsymbol{u}$ is the vector of inputs to the system (e.g., the wind speed), $\boldsymbol{y}$ is the vector of outputs (e.g., section loads at key locations of the system) and $\dot{(\cdot)}$ represents the time derivative. $\boldsymbol{X}$ and $\boldsymbol{Y}$ are the functions that return the derivative of the states and the outputs, respectively. We use the subscript 0 to indicate an equilibrium point (also called operating point) of the system, which satisfies Equation 1. The process of linearization consists of finding a linear model around this operating point. To obtain such model, each variable is expanded as: $\boldsymbol{x} = \boldsymbol{x}_0 + \delta\boldsymbol{x}$, $\boldsymbol{u} = \boldsymbol{u}_0 + \delta\boldsymbol{u}$, etc., where δ represents a small perturbation. Inserting these expansions into Equation 1, performing a Taylor expansion to the first order, and using the fact that the operating point satisfies Equation 1 leads to:

$$\delta\dot{\boldsymbol{x}} = \boldsymbol{A}_0\delta\boldsymbol{x} + \boldsymbol{B}_0\delta\boldsymbol{u}, \qquad \delta\boldsymbol{y} = \boldsymbol{C}_0\delta\boldsymbol{x} + \boldsymbol{D}_0\delta\boldsymbol{u} \tag{2}$$

where $\boldsymbol{A}$, $\boldsymbol{B}$, $\boldsymbol{C}$, $\boldsymbol{D}$ are Jacobian matrices evaluated at the operating point:

$$\boldsymbol{A}_0 = \left.\frac{\partial \boldsymbol{X}}{\partial \boldsymbol{x}}\right|_0, \quad \boldsymbol{B}_0 = \left.\frac{\partial \boldsymbol{X}}{\partial \boldsymbol{y}}\right|_0, \quad \boldsymbol{C}_0 = \left.\frac{\partial \boldsymbol{Y}}{\partial \boldsymbol{x}}\right|_0, \quad \boldsymbol{D}_0 = \left.\frac{\partial \boldsymbol{Y}}{\partial \boldsymbol{u}}\right|_0 \tag{3}$$

Matrices are linear operators, and therefore Equation 2 is a linear representation of the system about the operating point. Linear systems are simpler and computationally efficient, and they can be used in many applications, such as frequency-domain analyses, controller design, and stability analyses. An eigenvalue analysis of the state matrix $\boldsymbol{A}$ provides the mode shapes, natural frequencies, and damping of the system, which is relevant to study the stability of the system. The Jacobian matrices presented in Equation 3 can be computed using analytical gradients (if a simple and closed-form expression of $\boldsymbol{X}$ and $\boldsymbol{Y}$ is available), using finite-differences, or using a mix of the two.

Wind turbines are modeled as nonlinear systems, and the approach just described can be applied to linearize the model. Unfortunately, most numerical models of a wind turbine contain states both in fixed and rotating frames of reference. Additionally, the linear system obtained through linearization is periodic. A stable wind turbine under steady inputs reaches a periodic operating point, with a period corresponding to the inverse of the rotor speed. OpenFAST and HAWCStab2 address these two problems with the same approach, namely, the combination of applying the multi-blade coordinate (MBC) transformation method [15] for the former (to express all states in the fixed frame) and of modeling an isotropic rotor for the latter (to eliminate the periodicity). The MBC method only works for rotors with three or more blades, whereas the isotropic rotor is achieved by assuming no gravity, no skewed inflow, no shear, and no nacelle tilt angle. In addition, the inflow is modelled always perpendicular to the rotor axis, irrespective of any rotation such as the one generated by the deformation of the tower.

2.2 OpenFAST

OpenFAST uses a trimming algorithm to find a periodic steady state. The trimming algorithm works by minimizing the residual of rotor speed below a user-specified value. Convergence is achieved when the states and outputs across an entire period are within a given tolerance of the ones of the previous period. Currently, the trimming is achieved using time stepping with optional additional damping, which helps reduce the length of the transients and saves computational time. Note that additional damping is needed to achieve convergence in unstable configurations. The trimming algorithm includes a simple proportional controller, which either adjusts the generator torque (below rated wind speed), the pitch angle (above rated wind speed), or the yaw angle, to reach the desired rotational speed for a given steady uniform wind speed. The linear models are post-processed using the MBC transformation implemented in a Python script [22].

The linearization process of OpenFAST is more advanced than a standard linearization process, and the underlying nonlinear equations of OpenFAST include algebraic constraint equations. In that case, the linearization step requires the computation of additional Jacobian terms with respect to the constraint variables and equations, whereby the constraints are algebraically eliminated once linearized. A further complication arises due to the fact that OpenFAST uses a modular framework, where the modules are coupled through constraints that relate the inputs and outputs across modules. The linearization step is such that each module of OpenFAST performs its module-level linearization using the process outlined above (including algebraic constraints, where relevant). The coupling constraints in the OpenFAST glue code are also linearized, and then the linear models of each module and glue code are assembled together to form the full-system matrices. The assembly step requires the computation of Jacobian matrices that relate the input and output interconnections between each module.

OpenFAST supports linearization for quasi-steady airfoil or unsteady aerodynamics models, and for frozen, quasi-steady, or dynamic inflow models (which introduces aerodynamic states in addition to structural states). Note that OpenFAST can perform the linearization at different azimuthal positions across the periodic steady state to avoid the isotropic rotor assumption. However, we observed that the averaging of the linearized matrices across azimuthal angles returned inconsistent predictions. Therefore, the results presented in this paper are obtained by modeling the rotor as isotropic.

2.3 HAWCStab2

HAWCStab2 is the aeroservoelastic stability tool for three-bladed horizontal-axis wind turbines developed and released by DTU Wind Energy. The software has a wide range of uses, including the calculation of steady states, the run of modal analyses, and the tuning of control parameters. HAWCStab2 supports the same aerodynamic linearization options of OpenFAST. Blades can be modeled either as Timoschenko beams or as anisotropic beams that take as input fully populated stiffness and inertia matrices. The aeroelastic equations have been derived in a co-rotational formulation and then analytically linearized [13], which allows HAWCStab2 to perform aeroelastic stability analyses very efficiently. Stability can be analyzed via three types of eigenanalyses: structural only, aeroelastic, and aeroservoelastic. One of the most useful aspects of HAWCStab2 is the ability to animate mode shapes, simplifying the identification of the complicated modes that occur in modern, flexible wind turbines.

3 Aeroelastic stability of the IEA 15-MW reference wind turbine

The IEA15MW is an offshore reference wind turbine designed by a consortium of organizations within IEA Wind Technology Collaboration Programme Task 37 on systems engineering [21]. The turbine has a rotor diameter of 242 m and a hub height of 150 m, and it is mounted either on a monopile or on a floating substructure. This study adopts a simplified approach and models the tower as clamped at its base, which

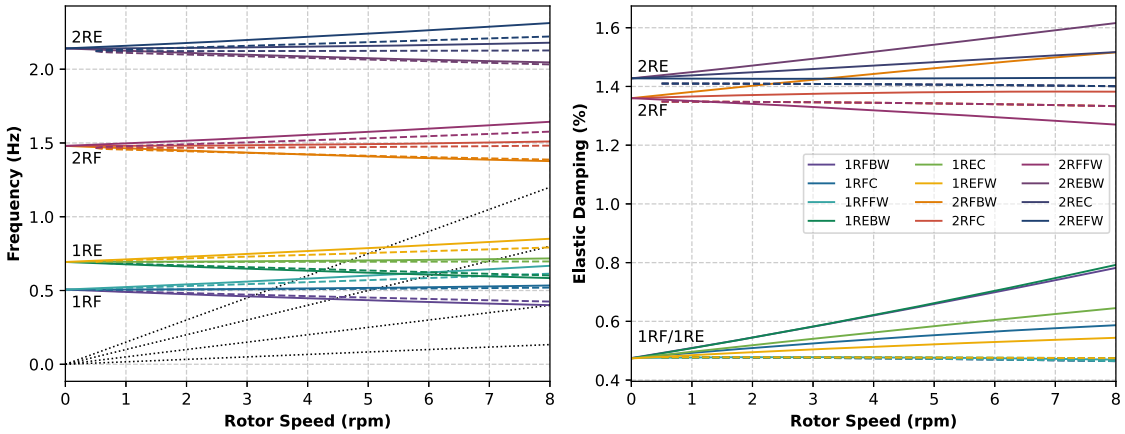

Figure 1: Natural frequencies and elastic damping ratios of the IEA 15-MW wind turbine rotor across a sweep of rotor speeds without aerodynamics. Solid lines show results from OpenFAST, dashed lines show results from HAWCStab2. Legend: 1/2 = order of mode, RF/RE = rotor flap/edge, BW/C/FW = backward whirling/collective/forward whirling.

is at 15 m above the mean sea level, therefore neglecting the offshore substructure of the system and, in practice, modeling a land-based machine. Note that the design of the turbine has been refined over the years, and each design iteration is marked with a tag number. This study models design iteration v1.1.10. A prior verification study between OpenFAST and the time-domain multibody solver HAWC2, using the IEA15MW in both steady-state and time-domain settings, focused on load comparisons [23]. This new effort extends the previous work by focusing on the aeroelastic stability of the machine. The fully populated stiffness and inertia matrices of the blades of the IEA15MW are recomputed with the open-source codes SONATA and ANBA4 [24], and a newly coded Python-based converter ensures that the HAWCStab2 and OpenFAST input data are as consistent as possible [22].

The comparison between OpenFAST and HAWCStab2 is performed in steps of increasing complexity. The next subsections discuss the different steps. It is important to note that results are expressed in terms of natural frequencies, ω_0, which are different from the damped frequencies, ω_d, especially for highly damped modes. The two are related by

$$\omega_d = \omega_0 \cdot \sqrt{1 - \zeta^2} \tag{4}$$

where ζ is the damping ratio. Note that this equation is only valid for ζ between 0 and 1. By default, the post-processing tool of OpenFAST generates natural frequencies, whereas HAWCStab2 returns damped frequencies. In the next subsections, solid lines correspond to results from OpenFAST and dashed lines correspond to results from HAWCStab2.

3.1 Rotor elastic response

The first analysis compares natural frequencies and elastic damping for a rotor without aerodynamics mounted on an infinitely stiff structure. Figure 1 shows the comparison for the first two flap and edge modes in terms of natural frequencies and elastic damping between the two solvers. Rotors are modeled in a fixed-free configuration in both solvers by prescribing the rotor speed. Blade pitch angle is kept at 0 deg. The match is satisfactory at lower rotor speeds, although lines diverge slightly as rotor speed increases. Also, a notable difference emerges in the lines of elastic damping, which tend to diverge between the two tools as rotor speed increases. Elastic damping in HAWCStab2 is not influenced by rotor speed, whereas it is in OpenFAST.

An additional comparison was run setting the rotor speed to rated and varying the blade pitch angle between -180 degrees and 180 degrees. The comparison in terms of natural frequencies and elastic damping (not shown) was satisfactory, with limited variations of the modal parameters with the pitch angle.

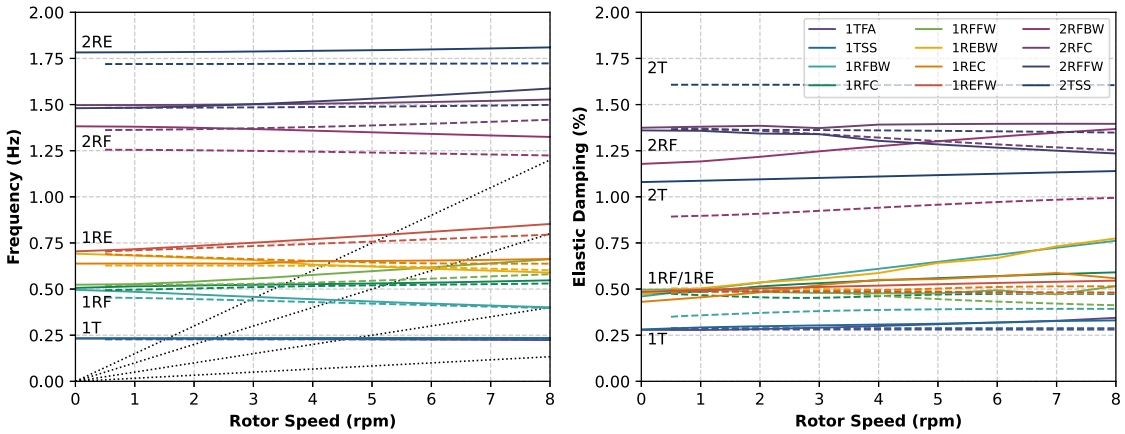

Figure 2: Natural frequencies and elastic damping ratios of the IEA 15-MW wind turbine across a sweep of rotor speeds without aerodynamics, with tower torsion in HAWCStab2 only. Solid lines show results from OpenFAST, dashed lines show results from HAWCStab2. Legend: 1/2 = order of mode, TSS/TFA = tower side-side/fore-aft, RF/RE = rotor flap/edge, BW/C/FW = backward whirling/collective/forward whirling.

3.2 Tower and rotor elastic response

The second analysis investigates the elastic response of the turbine accounting for the flexibility of both rotor and tower, again without aerodynamics. Here, two different comparisons were conducted. In the first one, not reported here for brevity, the tower in HAWCStab2 was modeled as torsionally stiff to account for the current limitation of OpenFAST that neglects tower torsion in its ElastoDyn module. Figure 2 includes the second comparison, where HAWCStab2 includes the effects of tower torsion. The comparison between OpenFAST and HAWCStab2 is again satisfactory, although differences in both natural frequencies and damping grow compared to the rigid tower results presented in Section 3.1. The effect of tower torsion is visible in the offset in the second rotor flapwise modes. Note that it would be possible to circumvent this limitation of OpenFAST by tuning the yaw spring and damper or by modeling the tower in the module SubDyn. Future development efforts will include the tower torsional response in ElastoDyn.

3.3 Tower and rotor aeroelastic response

The third and last comparison focuses on the full aeroelastic response, this time limited to quasi-steady aerodynamics (frozen wake and quasi-steady airfoil). Simulations are run at varying rotor speed and pitch angle, see Figure 3. Figure 4 shows the results as a function of wind speed. A satisfactory match in terms of natural frequencies and aeroelastic damping of first tower modes and first blade edgewise modes is observed. Flap modes are highly damped and are not identified by either code, except for the first rotor flapwise backward whirling mode (1RFBW) that is identified by OpenFAST. A noticeable discrepancy is again observed in the natural frequencies of the second rotor flapwise modes (2RF), where HAWCStab2 predicts lower frequencies than OpenFAST. Aeroelastic damping lines do not overlap, but are fairly close to each other across the range of wind speeds. The discrepancy is attributed to the lack of the torsional degree of freedom of the tower in OpenFAST and will be further investigated.

Work is ongoing to extend the comparison to account for the effects of unsteady airfoil aerodynamics and dynamic inflow. Although it is straightforward to generate predictions in both models, the manual mode identification approach used in the post-processing routines of OpenFAST [22] currently makes this task prohibitively cumbersome for the user. Preliminary results quantifying the impact of the dynamic inflow and unsteady airfoil aerodynamics modeling the blades as simple Euler-Bernoulli beams are given in Branlard et al. [26]. Work is ongoing to automate the mode identification in the post-processing of OpenFAST based on a modal assurance criterion. The comparison will also be extended to account for the monopile and the floater and the corresponding hydrodynamic effects.

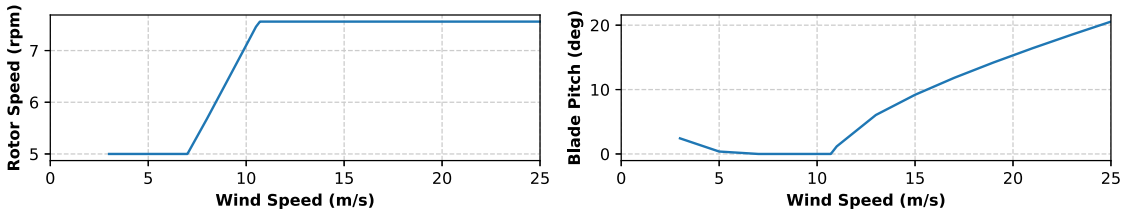

Figure 3: Schedule of rotor speed and blade pitch angle as a function of wind speed. This regulation trajectory was used in the aeroelastic comparison discussed in Section 3.3.

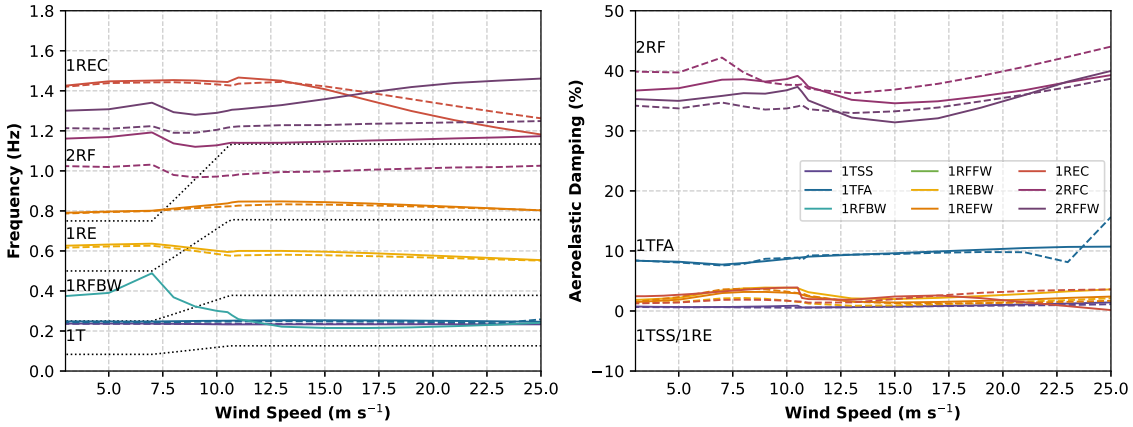

Figure 4: Natural frequencies and aeroelastic damping ratios of the IEA 15-MW wind turbine across a sweep of wind speeds. The linearization was performed with quasi-steady aerodynamics. Solid lines show results from OpenFAST, dashed lines show results from HAWCStab2. Legend: 1/2 = order of mode, TSS/TFA = tower side-side/fore-aft, RF/RE = rotor flap/edge, BW/C/FW = backward whirling/collective/forward whirling.

4 Aeroelastic stability and design of highly flexible rotors using OpenFAST

The last section of the paper focuses on the aeroelastic stability of a land-based wind turbine modeled in OpenFAST. The design was developed within the BAR project, which is funded by the U.S. Department of Energy to support the next generation of land-based wind turbines [1]. The BAR turbine platform has a nameplate power of 5 MW and a rotor diameter of 206 m, generating a specific power of 150 W m^{-2}. The hub height is set at 140 m. Within BAR, the blades were designed with integrated and multi-fidelity design capabilities, but the aeroelastic stability, based on linearized models, was not part of the design process. Blades are monolithic and straight (no prebend or sweep), have a maximum chord of 4.75 m, adopt pultruded carbon-fiber in the spar caps, and have a mass of 41.2 tons.

Figure 5 shows the natural frequencies and the associated aeroelastic damping of the baseline design simulated with quasi-steady aerodynamics. All modes are positively damped, except for the three blade torsional modes that drop to -0.3% between 12 and 15 m s^{-1}. The next subsections present parametric studies quantifying the impact of some key inputs on the aeroelastic stability of the BAR wind turbine. Table 1 summarizes key results.

4.1 Structural damping

The first input parameter that was investigated is structural damping, which is a parameter notoriously hard to predict both numerically and experimentally [25]. The baseline design assumes target values of 3% of logarithmic decrement (log dec) for the damping of first flap and edge modes. In torsion, 6% is assumed. These values, which mirror values commonly seen in industrial applications, correspond to damping ratios ζ of 0.48% and 0.95%, respectively, and to stiffness proportional values μ of 3.1e-3, 1.9e-3, and 5.6e-4 in flap, edge, and torsional directions, respectively. The stiffness proportional damping

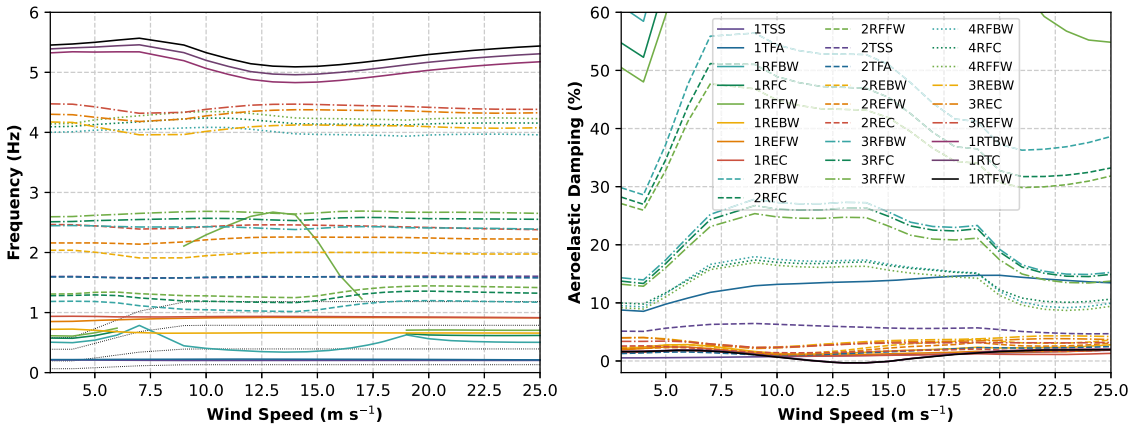

Figure 5: Natural frequencies and aeroelastic damping ratios of the BAR wind turbine across a sweep of wind speeds as obtained with OpenFAST adopting quasi-steady aerodynamics. Legend: 1(solid)/2(dashed)/3(dash-dotted)/4(dotted) = order of mode, TSS/TFA = tower side-side/fore-aft, RF/RE/RT = rotor flap/edge/torsion, BW/C/FW = backward whirling/collective/forward whirling.

formulation of BeamDyn makes damping increase with frequency for the higher order modes (see Figure 1 for an example). Decreasing the value of torsional structural damping to 3% log dec widens the range of wind speed where torsional modes are negatively damped. Torsional modes are now negatively damped between 11 and 16 m s^{-1} and drop to -0.9%. Further decreasing the values of structural damping to 1% log dec strengthens the negative damping of the torsional modes, which start going negative at 8 m s^{-1} and drop to -1.5%.

Next, we compared damage equivalent loads (DELs) of blade root moments for a Class A turbulent wind at 13 m s^{-1}. As expected, flap moments are fairly insensitive to structural damping, whereas the DELs of the torsional moment grow by 42.3% for a 3% torsional log dec and by 198.4% for a 1% log dec in the three directions. Edgewise moments are less sensitive, and do not grow for a 3% torsional log dec, whereas grow by 4.8% for a 1% log dec in the three directions. This analysis, although simplified, finds a good match between linearized and time-domain results. The analysis also highlights the need for predictive numerical tools to accurately estimate the structural damping of wind turbine blades.

4.2 Torsional stiffness

Torsional stiffness was identified as the strongest lever to prevent instabilities by Verdonck et al. [4]. Here, we varied torsional stiffness by perturbing the baseline value of shear stiffness (G) of the triaxial glass fiber composite, which is adopted in the outer and inner shell skins of the blade along its entire span [1]. A variation of -20% from the baseline value of 8.2 GPa worsens the instability of the torsional modes, whose aeroelastic damping drops to -1.0% between 11 and 15 m s^{-1}. The DEL of the torsional moment at blade root at 13 m s^{-1} grows by 15.9%. On the opposite, an increase of 20% in G makes the aeroelastic damping of the torsional moment positive across the entire operating range of the turbine. This analysis highlights the high sensitivity of composite material selection on the aeroelastic stability of various designs. For example, the biaxial glass in the BAR blade has a G that is 61% higher than in the triaxial composite (but only 39% of Young's modulus in the main fiber direction). Note also that blade torsional stiffness can always be increased by increasing the number of plies in the skin, although this change will lead to a mass and cost penalty.

4.3 Spanwise segmentation

A third sensitivity study was run adding a spanwise joint with a mass of 2,000 kg at 70% blade span [1]. The Campbell diagram shows a smaller impact of the added mass compared to the two previous studies. However, the added mass helps, and the segmented blade design no longer has any negatively damped mode. The DELs in edge and torsion grow by 24.3% and 26.7%, respectively, but the increase is caused by the added gravity loads and not by aeroelastic instabilities.

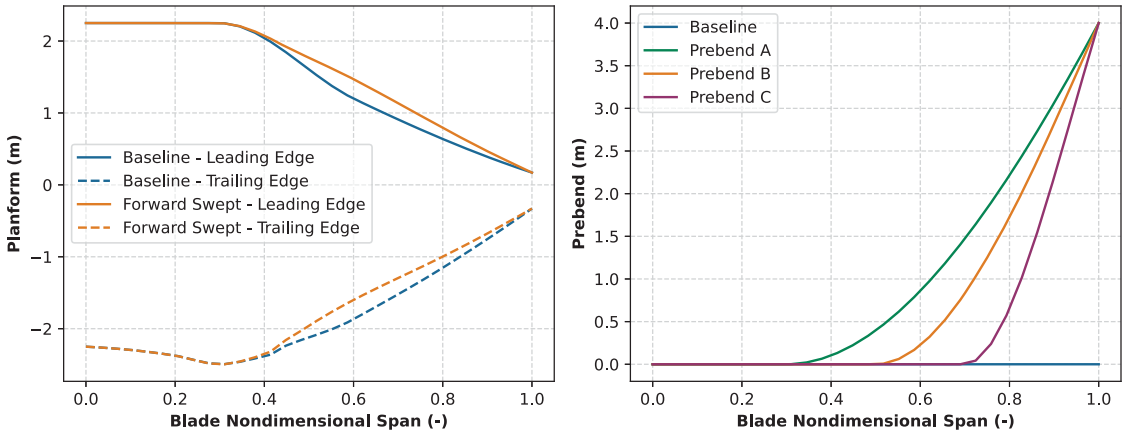

Figure 6: Planforms (left) and prebend distributions (right) used in the parametric studies described in Sections 4.4 and 4.5.

Design	Min ζ (%)	ΔDEL_E (%)	ΔDEL_T (%)
Baseline	−0.3	-	-
§4.1 - 3% log dec torsion	−0.9	+0.0	+42.3
§4.1 - 1% log dec	−1.5	+4.8	+198.4
§4.2 - G−20%	−1.0	+1.0	+15.9
§4.2 - G+20%	+0.2	−0.7	−6.8
§4.2 - G+20% and 3% log dec torsion	−0.4	−0.6	+0.3
§4.3 - Segmentation	0.0	+24.3	+26.7
§4.4 - Forward Swept	−0.2	−0.4	+6.7
§4.5 - Prebend A	−0.3	−2.7	−23.2
§4.5 - Prebend B	−0.3	−3.5	−21.4
§4.5 - Prebend C	+0.1	−3.7	−23.9

Table 1: Minimum damping ratio ζ and differences in the damage equivalent loads of the edgewise (ΔDEL_E) and torsional (ΔDEL_T) blade root moments for a turbulent wind at 13 m s^{-1} average speed across the design perturbations of the BAR rotor described in Section 4.

4.4 Airfoil chordwise placement

A fourth sensitivity study investigated the impact of the chordwise placement of the airfoils along the blade span. The baseline was varied, moving the leading edge forward and effectively introducing some limited amount of forward sweep into the blade design. The baseline and new planforms are shown in the left plot of Figure 6. The new planform has the same chord of the baseline design and the same spar cap and shear web positions in the blade root coordinate system. Although these blades share many parameters, the aeroelastic damping of the edgewise modes is different, and the new forward-swept design has first and second edgewise modes with an aeroelastic damping dangerously low at 0.3%, whereas the damping of these modes is at +0.8% in the baseline design.

4.5 Blade prebend

The fifth, and last, parametric study focused on the blade prebend. The baseline blade was designed to minimize logistic constraints and has no prebend [1]. Three different prebend distributions are tested, all with a tip value of 4 m (see the right plot in Figure 6). The three prebent blades generate fairly different Campbell diagrams (not reported here for brevity), with changes in frequencies and damping across edgewise and torsional modes growing from A to C. Interestingly, the aeroelastic damping of all modes of blade with prebend C is positive across wind speeds. DELs are reduced compared to the baseline design for all three prebend distributions.

5 Conclusions and future work

This work focuses on the aeroelastic stability of modern, slender, and flexible wind turbine rotors. We first perform a code-to-code benchmark study between the solvers HAWCStab2 and v3.5.3 of OpenFAST modeling quasi-steady aerodynamics. The two solvers are in strong agreement except for discrepancies in the second rotor flapwise modes. The differences are associated to the tower torsional flexibility and work is planned in OpenFAST to include tower torsion within its elastic model ElastoDyn. This comparison is actively being extended to quantify the effects of unsteady airfoil aerodynamics and unsteady rotor inflow. The comparison will also be extended to account for the offshore support structures.

We also present sensitivity analyses on the stability of a flexible land-based rotor design using OpenFAST. The design studies discussed in Section 4 confirm the very narrow stability margins currently available in flexible rotor designs. The initial design has a mild instability in the torsional modes, and the instability worsens when structural damping or blade torsional stiffness are reduced. The addition of a spanwise joint improves stability slightly, whereas the introduction of forward sweep causes the damping of the edgewise modes to drop. Lastly, we verified that aeroelastic stability is very sensitive to blade prebend. Overall, the parametric studies highlight the importance of aeroelastic stability analysis for modern wind turbine rotors. All design variables investigated in this paper have a notable impact on the aeroelastic solution, and automated design tools should integrate stability analysis to automatically design stable wind turbine rotors.

Acknowledgments

A portion of the research was performed using computational resources sponsored by the Department of Energy's Office of Energy Efficiency and Renewable Energy and located at the National Renewable Energy Laboratory. This work was authored in part by the National Renewable Energy Laboratory, operated by Alliance for Sustainable Energy, LLC, for the U.S. Department of Energy (DOE) under Contract No. DE-AC36-08GO28308. Funding provided by the U.S. Department of Energy Office of Energy Efficiency and Renewable Energy, Wind Energy Technologies Office. The views expressed in the article do not necessarily represent the views of the DOE or the U.S. Government. The U.S. Government retains and the publisher, by accepting the article for publication, acknowledges that the U.S. Government retains a nonexclusive, paid-up, irrevocable, worldwide license to publish or reproduce the published form of this work, or allow others to do so, for U.S. Government purposes.

Code and Data Availability

The following links are repositories available at https://github.com. The design v1.1.10 of the IEA 15 RWT is available at IEAWindTask37/IEA-15-240-RWT. The BAR designs are available at NREL/BAR_Designs. v3.5.3 of OpenFAST is available at OpenFAST/openfast. The code for running the MBC3 and the OpenFAST to HAWC2 converter are available at OpenFAST/openfast_toolbox.

References

[1] Bortolotti P, Johnson N, Abbas NJ, Anderson E, Camarena E, and Paquette J. Land-based wind turbines with flexible rail-transportable blades – Part 1: Conceptual design and aeroservoelastic performance. *Wind Energy Science*, 6:1277–1290, 2021. doi: 10.5194/wes-6-1277-2021

[2] Dillon MV, Kallesøe BS, Johnson S, Pirrung GR, Riva R, and Barnaud F. Large wind turbine edge instability field validation. *Journal of Physics: Conference Series*, 1618, 2020. doi: 10.1088/1742-6596/1618/5/052014

[3] Hach O, Verdonck H, Polman JD, Balzani C, Müller S, Rieke J, Hennings H. Wind turbine stability: Comparison of state-of-the-art aeroelastic simulation tools. *Journal of Physics: Conference Series*, 1618, 2020. doi: 10.1088/1742-6596/1618/5/052048

[4] Verdonck H, Hach O, Polman JD, Braun O, Balzani C, Müller S, and Rieke J. Uncertainty quantification of structural blade parameters for the aeroelastic damping of wind turbines: a code-to-code comparison. *Wind Energy Science Discussion*, in review, 2023. doi: 10.5194/wes-2023-80

[5] Theodorsen T. General theory of aerodynamic instability and the mechanism of flutter. *NACA Technical Report*, 1949.

[6] Lobitz DW. Aeroelastic stability predictions for a MW-sized blade. *Wind Energy*, 7:211-224, 2004. doi: 10.1002/we.120

[7] Owens BC, Griffith DT, Resor BR, Hurtado JE. Impact of modeling approach on flutter predictions for very large wind turbine blade designs. *SAND2013-3108C*, 2013.

[8] Pourazarm P, Modarres-Sadeghi Y, Lackner M. A parametric study of coupled-mode flutter for MW-size wind turbine blades. *Wind Energy*, 19: 497–514. 2016. doi: 10.1002/we.1847

[9] Griffith DT, Chetan M. Assessment of flutter prediction and trends in the design of large-scale wind turbine rotor blades. *Journal of Physics: Conference Series*, 1037(4), 2018. doi: 10.1088/1742-6596/1037/4/042008

[10] Kelley CL, Paquette J. Investigation of flutter for large, highly flexible wind turbine blades. *Journal of Physics: Conference Series*, 1618, 2020. doi: 10.1088/1742-6596/1618/5/052078

[11] Chetan M, Yao S, Griffith DT. Flutter Behavior of Highly Flexible Two- and Three-bladed Wind Turbine Rotors. *Wind Energy Science*, 7:1731–1751, 2021. doi: 10.5194/wes-7-1731-2022

[12] Hansen MH. Aeroelastic stability analysis of wind turbines using an eigenvalue approach. *Wind Energy*, 7:133-143, 2004. doi: 10.1002/we.116

[13] Hansen MH. Aeroelastic Properties of Backward Swept Blades. *49th AIAA Aerospace Sciences Meeting including the New Horizons Forum and Aerospace Exposition*, 2011. doi: 10.2514/6.2011-260

[14] Tibaldi C, Kim T, Larsen TJ, Rasmussen F, de Rocca Serra R, Sanz F. An investigation on wind turbine resonant vibrations. *Wind Energy*, 19:847–859, 2016. doi: 10.1002/we.1869

[15] Coleman RP and Feingold AM. Theory of self-excited mechanical oscillations of helicopter rotors with hinged blades. 1958.

[16] Bottasso CL, Cacciola S. Model-independent periodic stability analysis of wind turbines. *Wind Energy*, 18:865–887, 2015. doi: 10.1002/we.1735

[17] Riva R, Cacciola S, Bottasso CL. Periodic stability analysis of wind turbines operating in turbulent wind conditions. *Wind Energy Science*, 1:177–203, 2016. doi: 10.5194/wes-1-177-2016

[18] Stäblein AR, Hansen MH, Verelst DR. Modal properties and stability of bend–twist coupled wind turbine blades. *Wind Energy Science*, 2:343–360, 2017. doi: 10.5194/wes-2-343-2017

[19] Riva R, Spinelli M, Sartori L, Cacciola S, Croce A. Stability analysis of wind turbines with bend-twist coupled blades. *Journal of Physics: Conference Series*, 1037(6), 2018. doi: 10.1088/1742-6596/1037/6/062014

[20] Jonkman JM, Jonkman BJ. FAST modularization framework for wind turbine simulation: full-system linearization. *Journal of Physics: Conference Series*, 753, 2016. doi: 10.1088/1742-6596/753/8/082010

[21] Gaertner E, et al. IEA Wind TCP Task 37: Definition of the IEA 15-Megawatt Offshore Reference Wind Turbine. *IEA Wind TCP Task 37 Technical Report*, 2020. doi: 10.2172/1603478

[22] `http://github.com/OpenFAST/openfast_toolbox`, Accessed on March 21st, 2024.

[23] Rinker J, Gaertner E, Zahle F, Skrzypiński W, Abbas N, Bredmose H, Barter G, Dykes K. Comparison of loads from HAWC2 and OpenFAST for the IEA Wind 15 MW Reference Wind Turbine 2020. *Journal of Physics: Conference Series*, 1618, 2020. doi: 10.1088/1742-6596/1618/5/052052

[24] Feil R, Pflumm T, Bortolotti P, Morandini M. A cross-sectional aeroelastic analysis and structural optimization tool for slender composite structures. *Composite Structures*, 253, 2020. doi: 10.1016/j.compstruct.2020.112755

[25] Kliem M. Damping of Composite Mast Structures. *DCAMM Special Report*, No. S240, 2018.

[26] Branlard E, Jonkman B, Pirrung GR, Dixon K, Jonkman J. Dynamic inflow and unsteady aerodynamics models for modal and stability analyses in OpenFAST. *Journal of Physics: Conference Series*, 2265, 2022. doi: 10.1088/1742-6596/2265/3/032044